

## Unified analysis of absolute and convective instabilities in stimulated Compton Raman scattering and free-electron lasers

B. Steinberg, A. Gover, and S. Ruschin

*Department of Electron Devices and Materials and Electromagnetic Radiation, Faculty of Engineering, Tel-Aviv University,  
69978 Ramat Aviv, Israel*

(Received 21 June 1985)

Parametric instabilities in the interaction between a cold-electron beam, a static or electromagnetic pump, and a scattered (signal) electromagnetic wave are studied. The interaction schemes are classified according to the mutual sense of propagation of the waves and the beam. The unified analysis yields the known convective and absolute slow-plasma-wave instabilities [forward- and backward-wave free-electron lasers (FEL)]. In addition, we identify the possibility of convective and absolute fast-plasma-wave instabilities. Analysis and numerical computation of gain and oscillation in both known and new instability mechanisms are performed in the framework of a general model beyond the range of previously reported studies. A general approximate threshold condition expression for all the possible absolute instabilities is given. All of these instabilities may appear in practical schemes like FEL oscillators as parasitic effects. Their relative importance is considered by means of numerical examples.

### I. INTRODUCTION

There have been a number of previous theoretical investigations of the backward-wave absolute instability in the cold beam, one-dimensional magnetostatically pumped free-electron laser (FEL). Liewer *et al.*<sup>1</sup> showed that this instability requires contradirectional group velocities of the beam and the em signal, and calculated a threshold interaction length or pump strength for the instability. Cary and Kwan investigated this instability numerically and analytically,<sup>2,3</sup> and by arguing that the excited wave depletes energy from the beam, calculated an upper limit for its saturation level.<sup>2</sup> Liewer, Lin, Dawson, and Caponi showed in a particle-simulation study of the magnetostatically pumped FEL that this long-wave absolute instability may sometime dominate the FEL device (Ref. 4, Sec. V).

Our purpose in the present paper is to describe the FEL beam instability problem in a more general framework of parametric interaction analysis, allowing the pump (wiggler) to be either static or time varying (electromagnetic). Stability of the beam in the presence of an electromagnetic pump is of interest because FEL's with an em pump are currently considered in various experimental designs, and also because the circulating radiation power in a high-intensity static wiggler FEL oscillator may behave as a secondary em pump (wiggler) for absolute instabilities in the beam.

The consideration of the more general (electromagnetic pump) case has also a more far-reaching ramification. It reveals that, in the general case two different kinds of absolute instabilities can exist in the beam—one involving interaction with the slow (negative-energy) plasma wave and the other involves interaction with the fast (positive-energy) plasma wave. While the first kind (slow-wave instability) can take place with either static or em pump, the

second kind (fast-wave instability) cannot take place at all with a static pump and would be exposed only with a general description of the pump as taken in the present analysis.

The instability analyzed by<sup>1</sup> for the static pump is the slow-wave instability, while the fast-wave instability was partly analyzed before in Ref. 5 (only for the specific example of an electromagnetic pump moving at the speed of light in the electron-beam propagation direction) and was considered there erroneously as a slow-wave instability. These two contradirectional interaction oscillation schemes (absolute instabilities) are identified and classified in Sec. II along with the codirectional interaction FEL amplifiers (convective instabilities) of the system, thus revealing all the parametric instability schemes that are possible in a general FEL structure consisting of two electromagnetic waves and an electron beam. The threshold conditions of the two absolute instabilities are different from each other, they are calculated and compared in Sec. V.

In addition to the generalization to electromagnetic pump and fast-wave instabilities the model taken in the present paper is more general than the previous papers in the following respects. (a) The wiggler field may be strong to the extent that the quiver velocity is relativistic ( $a_w = eA_w/mc \cong 1$ ). (b) The highly relativistic limit is not taken. (c) The wiggler and signal may have arbitrary polarization and phase velocity. (d) The beam cross section is finite. (e) In order to keep the analysis applicable to most optical-wavelength FEL's the collective (space-charge-dominated regime) limit  $\bar{\theta}_p = \omega'_p L / V_{0z} \gg 1$  is not assume *a priori* in the analysis, but we take this limit further on in order to obtain analytic expressions. We also assume this limit in the qualitative discussion of Sec. II for the purpose of exposing the fundamental physical processes underlying the instability effects.

## II. QUALITATIVE DESCRIPTION OF INSTABILITIES

In this section we provide qualitative explanation and classification of all the instability schemes possible in the general FEL structure. The model taken to describe the FEL structure in this section allows a static or em wiggler field of arbitrary propagation direction and phase velocity. The generated signal field is any transverse em wave in an  $e$ -beam-loaded waveguide or open space. The  $e$  beam is assumed to be in the space-charge-dominated regime  $\bar{\theta}_p \gg 1$ , where  $\bar{\theta}_p = \omega'_p L / V_{0z}$  is the space-charge parameter,  $\omega'_p = [e^2 n_0 / (\epsilon_0 m \gamma_z^2 \gamma_0)]^{1/2}$  is the longitudinal plasma frequency of the  $e$  beam, and  $L / V_{0z}$  is the interaction-region transit time. Taking this limit allows us to discuss the parametric interaction in terms of the collective eigenmodes of the beam: the slow and fast space-charge waves. Nevertheless, the quantitative analysis of the next section is not bound to this limit.

Figures 1 and 2 describe the various interaction schemes in the FEL structure according to two different cross sections of classification. Figure 1 classifies the interaction schemes according to the wiggler- and signal-wave propagation directions relative to each other and to the beam. The interaction is viewed as general distributed parametric interaction schemes in a nonlinear medium (like Raman scattering in matter). The nonlinear medium is the  $e$  beam, and since it is an unisotropic medium, four different schemes are possible: two [Figs. 1(a) and 1(b)] are backward Raman scattering schemes and the other two [Figs. 1(c) and 1(d)] are forward Raman scattering schemes. "Forward" and "backward" are used here in the sense that the scattered wave (signal) propagates in the same or in the counter direction to the pump (wiggler) wave, respectively.

Figure 2 describes an alternative cross section of classification. It depicts the Stokes diagrams of the various interaction schemes classified according to the kind of idler wave (space-charge wave) with which the interaction takes place and according to the relative orientations between the signal- and the idler-wave group velocities. This is a more significant classification, because in the linear non-depleted pump model used here, only the characteristics of the interacting idler and signal waves determine the nature of the interaction.

It is well known that when the signal and idler waves are carrying energy in counter directions, a contradirectional distributed feedback mechanism is introduced, which can result in oscillation (absolute instability) if gain is available. On the other hand, when the two waves are codirectional, only amplification (convective instability) may be obtained. The contradirectional oscillation schemes are depicted in Figs. 2(b) and 2(c) while the codirectional convective instability FEL amplifier schemes are depicted by Figs. 2(a) and 2(d). In Figs. 2(a) and 2(c) the idler wave is the slow space-charge plasma wave and in Figs. 2(b) and 2(d) it is the fast space-charge wave. (Note that the group velocities of both space-charge waves are equal to the  $e$ -beam velocity  $+V_{0z}$ .)

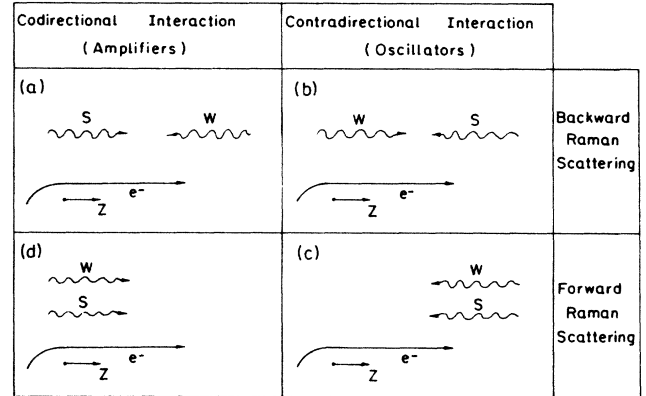


FIG. 1. Four basic scattering schemes: (a) backward Raman scattering amplifier (conventional FEL), (b) backward Raman scattering oscillator, (c) forward Raman scattering oscillator, (d) forward Raman scattering amplifier.

In the Stokes diagram of Fig. 2 the wiggler is represented by corresponding arrows stretched between the space-charge wave and the signal-wave dispersion curves. These diagrams represent the conservation of energy and momentum conditions in the interaction between the elementary excitations of the system. Notice that all four interaction schemes take place only with the two intersection points of the lower displaced space-charge dispersion curve and the signal-wave dispersion curve. It is only where the wiggler arrow starts: upper and lower half-plane—corresponding to up or down conversion of the scattered radiation (signal) wave—which determines if the intersection point corresponds to the slow or fast space-charge wave, respectively. The slopes of the wiggler vectors are the phase velocities of the wiggler waves. Various phase velocities and wave orientations are depicted in Fig. 2, including slow waves ( $V_{ph} < c$ ), which are possible in slow-wave structures<sup>6</sup> and static pumps. The latter case is represented by horizontal arrows.

Inspection of Figs. 2(b) and 2(d) confirms that the down-conversion fast-wave instability diagrams cannot be generated at all with static pumps (horizontal vectors), in agreement with our observation in the Introduction.

Our analysis revealed that all the instabilities possible in a general FEL structure without beam prebunching are the ones given by Fig. 2. This includes the slow and the fast space-charge-wave convective instabilities (up-conversion and down-conversion FEL amplifier), depicted by 2(a) and 2(d), respectively, and the slow- and fast-wave absolute instabilities (up- and down-conversion oscillators) depicted by 2(c) and 2(b), respectively. In the absence of electron prebunching there are no instabilities involved with the other upper-two intersection points of the dispersion curves. A physical explanation of this result can be given using Fig. 3, which depicts the only two possible parametric processes between the elementary excitations of the system that can generate signal-wave photons (gain). The diagram 3(b) requires annihilation of a

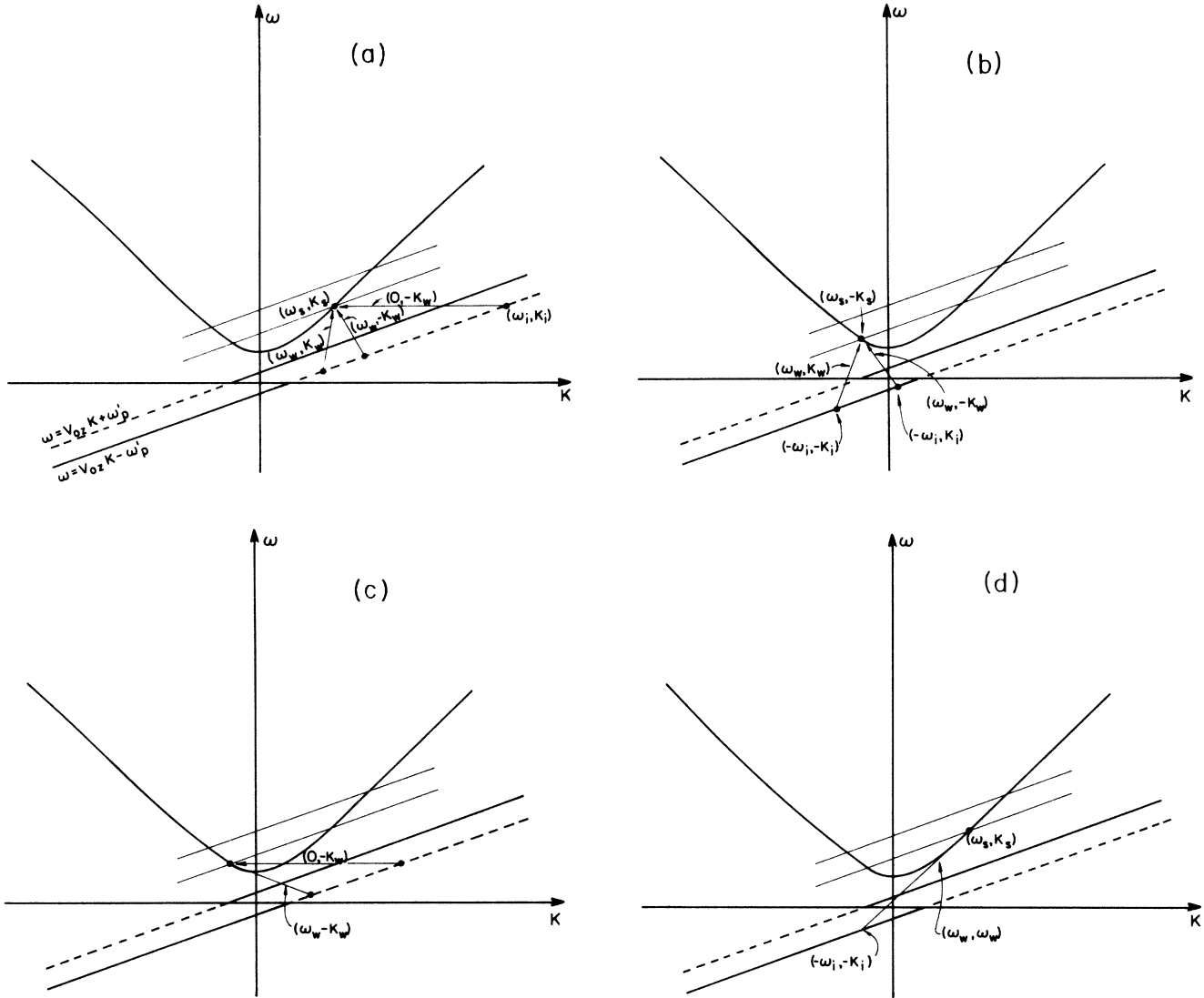


FIG. 2. Stokes diagrams (conservation of energy and momentum) for the scattering processes which are discussed in the present paper. The curve  $\omega^2=c^2k^2+\omega_{c0}^2$  represents the dispersion relation of the signal wave and the curves  $\omega=V_{0z}k\pm\omega'_p$  are the space-charge waves' dispersion relation. Note that the solid lines correspond to the fast (positive-energy) space-charge waves, and the dashed lines correspond to the slow (negative-energy) space-charge waves. (a) Slow space-charge wave convective instabilities, (b) fast space-charge wave absolute instabilities (contradirectional interaction), (c) slow space-charge wave absolute instabilities (contradirectional interaction), (d) fast space-charge wave convective instability.

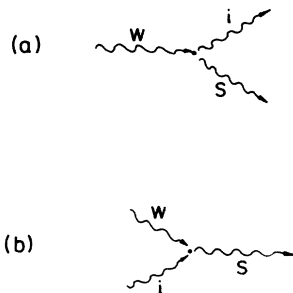


FIG. 3. Feynman diagrams, showing the photon-plasmon scattering processes: (a) one wiggler photon is annihilated, a signal photon and a plasmon are created. (b) one wiggler photon and one plasmon are annihilated, and a signal photon is created. This process is possible only if the electron beam is prebunched.

wiggler photon and an idler plasmon to generate a signal photon. This is not possible in a beam without prebunching, where plasmons are not inserted and therefore this diagram is ruled out all together (the prebunched-beam FEL is considered elsewhere<sup>7</sup>). We thus consider only diagram 3(a) and write down its corresponding energy-conservation conditions for the respective cases of fast and slow plasmons' generation:  $\hbar\omega_w = \hbar\omega_f + \hbar\omega_s$ ,  $\hbar\omega_w = (-\hbar\omega_{sl}) + \hbar\omega_s$  (note that the slow plasmon has negative energy  $-\hbar\omega_{sl}$ ). These relations dictate down conversion of the signal-wave frequency when gain is obtained by coupling to the fast space-charge wave, and up conversion in the opposite case. It can be seen that only the two lower intersection points of the dispersion curves of Fig. 2 satisfy these conditions, whatever the wiggler vector is chosen to be.

Each Raman scattering scheme described in Fig. 1 has corresponding Stokes diagrams in Fig. 2. A detailed discussion of all possible instabilities in the general FEL system in terms of the Fig. 1 and Fig. 2 diagrams classification is given in Appendix A. The instabilities which are previously known or are of special interest are the following.

(1) The conventional magnetostatic and electromagnetic pump FEL's (convective instability) are depicted by Fig. 1(a) and by the horizontal and left-going wiggler arrows of Fig. 2(a).

(2) The electromagnetically pumped fast-plasma-wave contradirectional interaction oscillation (absolute instability) which was analyzed before by Gover<sup>5</sup> is depicted by Fig. 1(b) and by the right-going vector of Fig. 2(b). It is shown that this same instability can also be excited by the configuration depicted by Fig. 1(c) and the left-going arrow of Fig. 2(b).

(3) The magnetostatically pumped slow-plasma-wave contradirectional interaction oscillation (absolute instability) which was analyzed before by Liewer *et al.*<sup>1,4</sup> and Carry *et al.*<sup>2,3</sup> is depicted by Fig. 1(c) and the horizontal vector of Fig. 2(c).

(4) Various electromagnetically pumped forward Raman scattering schemes [Figs. 1(c) and 1(d)] were found capable of producing absolute or convective instabilities. These schemes are closely related (inverse processes) to the plasma heating and electron-acceleration schemes analyzed before by Rosenbluth *et al.*,<sup>8</sup> Cohen<sup>9</sup> and others. In the FEL schemes they are usually of little practical interest as devices since they produce signal waves of frequency very close to the pump frequency. However, they should be of some concern in FEL oscillators design, since they may also be sources of parasitic instabilities.

Finally, we add a clarifying comment regarding terminology. The term backward-wave oscillation is frequently used in the literature in the sense of oscillation by means of contradirectional interaction feedback mechanism.<sup>10</sup> This should be distinguished from the terms forward and backward scattering used in this paper. For example, Fig. 2(b) depicts a contradirectional ("backward-wave") fast space-charge oscillation mechanism, but it can be obtained by both forward and backward Raman scattering schemes.

### III. QUANTITATIVE ANALYSIS

In the quantitative analysis we make no *a priori* assumption which of the space-charge waves are involved in the interaction. Indeed, the analysis will apply even in the tenuous beam regime  $\bar{\theta}_p \ll 1$ , where there is no isolated coupling to one of the space-charge waves. A small-signal (linear gain) model is used to describe the electromagnetic waves and electron-beam current excitation.<sup>5,11</sup> The beam is assumed to be "cold" and thus can be described by fluid-plasma equations.

#### A. Backward Raman scattering schemes

We mark the wiggler and signal field by indices 1 (the wave which propagates in the same direction as the  $e$  beam,  $+z$ ) and 2 (the wave propagating in the direction

counter to the  $e$  beam,  $-z$ ). The fields are

$$\begin{aligned} E_2^1(x, y, z) &= \text{Re}[C_2^1(z)\tilde{\mathcal{E}}_2^1(x, y)e^{\pm ik_2^1 z - i\omega_2^1 t}], \\ B_2^1(x, y, z) &= \text{Re}[C_2^1(z)\tilde{\mathcal{B}}_2^1(x, y)e^{\pm ik_2^1 z - i\omega_2^1 t}], \end{aligned} \quad (1)$$

where  $\tilde{\mathcal{E}}_2^1(x, y)e^{\pm ik_2^1 z - i\omega_2^1 t}$  and  $\tilde{\mathcal{B}}_2^1(x, y)e^{\pm ik_2^1 z - i\omega_2^1 t}$  are the fields of the empty waveguide modes and  $C_2^1(z)$  are the amplitudes of the waves in the presence of the beam.

The excitation equations for the wave amplitudes  $C_2^1(z)$  are derived from Maxwell equations<sup>12,13</sup>

$$\begin{aligned} \frac{dC_2^1(z)}{dz} &= \mp \frac{1}{4|\mathcal{P}_2^1|} e^{\mp ik_2^1 z} \\ &\times \int \int \tilde{\mathbf{J}}_{T2}^1(x, y, z) \cdot \tilde{\mathcal{E}}_{T2}^1(x, y) dx dy, \end{aligned} \quad (2)$$

where  $\tilde{\mathbf{J}}_2^1(x, y, z)$  are the current components at the frequencies of modes  $\tilde{\mathcal{E}}_2^1(x, y)$ ,  $T$  denotes the transverse components, and  $\mathcal{P}_2^1$  are the normalization powers of the electromagnetic modes:

$$\mathcal{P}_2^1 = \frac{1}{2} \text{Re} \int \int [\tilde{\mathcal{E}}_2^1 \times \tilde{\mathcal{H}}_2^{*1}] \cdot \hat{\mathbf{i}}_z dx dy. \quad (3)$$

The electromagnetic modes  $\tilde{\mathcal{E}}(x, y)$  may be waveguide modes or free-space modes (like Hermit-Gaussian modes) where in the latter case it is assumed that the interaction length  $L$  is shorter than a Rayleigh length. The modes may be of arbitrary polarization. The phase velocity of the waves  $\omega/k$  may have any value, including zero, which corresponds to a static wiggler (zero-frequency pump).

We now define the beat frequency  $\omega_i = \omega_1 - \omega_2$  and assume the presence of a density (idler) wave at the beat frequency:

$$\begin{aligned} n_i(\mathbf{r}, t) &= \text{Re}[\tilde{n}_i(x, y, z)e^{-i\omega_i t}] \\ &= \frac{1}{2} \tilde{n}_i(x, y, z)e^{-i\omega_i t} + \text{c.c.} \end{aligned} \quad (4)$$

We confine our discussion to purely transverse fields. Then the first-order response of the electron velocity is purely transverse:

$$\mathbf{V}_T(\mathbf{r}, t) = [\frac{1}{2} \tilde{\mathbf{V}}_{T1}(x, y, z)e^{-i\omega_1 t} + \frac{1}{2} \tilde{\mathbf{V}}_{T2}(x, y, z)e^{-i\omega_2 t}] + \text{c.c.} \quad (5)$$

These velocity fields give rise to transverse current components at the signal and wiggler frequencies. By substituting Eqs. (4) and (5) into the expression

$$\mathbf{J}_T = -en_i(\mathbf{r}, t)\mathbf{V}_T(\mathbf{r}, t)$$

and neglecting terms which are not oscillating with frequencies  $\omega_1, \omega_2$ , one finds that

$$\mathbf{J}_T = (\frac{1}{2} \tilde{\mathbf{J}}_{T1} e^{-i\omega_1 t} + \frac{1}{2} \tilde{\mathbf{J}}_{T2} e^{-i\omega_2 t}) + \text{c.c.}, \quad (6)$$

where

$$\tilde{\mathbf{J}}_{T1} = -\frac{1}{2} e \tilde{\mathbf{V}}_{T2} \tilde{n}_i,$$

$$\tilde{\mathbf{J}}_{T2} = -\frac{1}{2} e \tilde{\mathbf{V}}_{T1} \tilde{n}_i^*.$$

We now assume that the variation of all the fields

across the  $e$ -beam cross section is small. Consequently, when the total velocity field

$$\mathbf{V} = \hat{\mathbf{z}} V_{0z} + \left[ \frac{1}{2} \tilde{\mathbf{V}}_{T2}^{\perp}(x, y, z) e^{-i\omega_1 t} + \text{c.c.} \right]$$

is substituted in the first-order (in  $E, B$ ) transverse component of the Lorentz equation, the transverse velocity phasor equations results:

$$\left[ -i\omega_2 + V_{0z} \frac{\partial}{\partial z} \right] \tilde{\mathbf{V}}_{T2}^{\perp} = -\frac{e}{\gamma_0 m} \left[ \tilde{\mathbf{E}}_2^{\perp} + V_{0z} \hat{\mathbf{z}} \times \tilde{\mathbf{B}}_2^{\perp} \right],$$

where

$$\gamma_0 = \left[ 1 - \left( \frac{V}{C} \right)^2 \right]^{-1/2}.$$

Substituting Eqs. (1) in, we obtain explicit expressions for  $\tilde{\mathbf{V}}_{T2}^{\perp}$

$$\begin{aligned} \tilde{\mathbf{V}}_{T2}^{\perp}(\mathbf{r}) &= C_2^{\perp}(z) \tilde{\mathcal{V}}_{T2}^{\perp}(x, y) e^{\pm i k_2 z}, \\ \tilde{\mathcal{V}}_{T2}^{\perp}(x, y) &= -i \frac{e/\gamma_0 m}{\omega_2 \mp V_{0z} k_2} \\ &\quad \times \left[ \tilde{\mathcal{E}}_{T2}^{\perp}(x, y) + V_{0z} \hat{\mathbf{z}} \times \tilde{\mathcal{B}}_{T2}^{\perp}(x, y) \right], \end{aligned} \quad (7)$$

where  $V_{0z}$  is the axial dc electron velocity (in  $+z$  direction). By substituting Eq. (7a) in the excitation equations (2) we obtain

$$\begin{aligned} \frac{dC_1(z)}{dz} &= C_2(z) \frac{e}{8 |\mathcal{P}_1|} e^{-i(k_1 + k_2)z} \\ &\quad \times \int \int \tilde{\mathcal{V}}_{T2}^{\perp}(x, y) \tilde{n}_i(x, y, z) \cdot \tilde{\mathcal{E}}_{T1}^*(x, y) dx dy, \end{aligned} \quad (8)$$

$$\begin{aligned} \frac{dC_2(z)}{dz} &= -C_1(z) \frac{e}{8 |\mathcal{P}_2|} e^{i(k_1 + k_2)z} \\ &\quad \times \int \int \tilde{\mathcal{V}}_{T1}^{\perp}(x, y) \tilde{n}_i^*(x, y, z) \cdot \tilde{\mathcal{E}}_{T2}^*(x, y) dx dy. \end{aligned}$$

Equations (7b) and (8) describe the excitation of the em fields by the density modulation. We now turn to the inverse process and derive the excitation equations of the density wave  $\tilde{n}_i$  by the em fields. The density modulation  $\tilde{n}_i$  is generated by the ponderomotive force, which results in from second-order expansion of the Lorentz-force equation. First, we derive the longitudinal velocity modulation. The total velocity field in the  $z$  direction is (neglecting any transverse variation across the narrow beam)

$$V_z(\mathbf{r}, t) = V_{0z} + \left[ \frac{1}{2} \tilde{V}_{zi}(z) e^{-i\omega_1 t} + \text{c.c.} \right].$$

Substituting into the longitudinal component of the Lorentz-force equation expanded to second order results in

$$\begin{aligned} \left[ -i\omega_i + V_{0z} \frac{\partial}{\partial z} \right] \frac{1}{2} \tilde{V}_{zi}(z) e^{-i\omega_1 t} + \text{c.c.} \\ = -\frac{e}{\gamma_z^2 \gamma_0 m} [E_{SC}(z, t) + (V \times B) \cdot \hat{\mathbf{z}}]. \end{aligned} \quad (9)$$

$E_{SC}(z, t)$  is the longitudinal space-charge field generated by the density modulation,  $\gamma_z = (1 - \beta_z^2)^{-1/2} = \gamma_0 / (1 + \bar{a}_w^2)^{1/2}$ ,  $\bar{a}_w$  is the normalized rms transverse mechanical momentum of the electron in the wiggler field.<sup>11</sup> For a magnetostatic wiggler  $\bar{a}_w = e \bar{B}_w / mck_w$  may be in practice of the order of 1 (transverse relativistic regime) and thus not negligible. For electromagnetic pumps  $\bar{a}_w = e |\bar{A}_w| / mc \ll 1$  in most practical situations. The second forcing term is the ponderomotive "field," which using (1) and (7a) is given by

$$\begin{aligned} (\mathbf{V} \times \mathbf{B})_z &= \frac{1}{4} [(\tilde{\mathbf{V}}_{T1} e^{-i\omega_1 t} + \tilde{\mathbf{V}}_{T2} e^{-i\omega_2 t}) + \text{c.c.}] \\ &\quad \times [(\tilde{\mathbf{B}}_{T1} e^{-i\omega_1 t + ik_1 z} + \tilde{\mathbf{B}}_{T2} e^{-i\omega_2 t - ik_2 z}) + \text{c.c.}]. \end{aligned}$$

Taking only phasor components which oscillate as  $e^{-i\omega_i t}$  we get from Eq. (9)

$$\left[ -i\omega_i + V_{0z} \frac{\partial}{\partial z} \right] \tilde{V}_{zi} = \frac{-e}{\gamma_z^2 \gamma_0 m} (\tilde{E}_{SC} + \tilde{E}_{pond}^{\omega_i}), \quad (10)$$

where

$$\begin{aligned} \tilde{E}_{pond}^{\omega_i} &= C_2^*(z) C_1(z) \tilde{\mathcal{E}}_{pond}^{\omega_i} e^{i(k_1 + k_2)z}, \\ \tilde{\mathcal{E}}_{pond}^{\omega_i} &= \frac{1}{2} [\tilde{\mathcal{V}}_{T1}^{\perp}(x, y) \times \tilde{\mathcal{B}}_{T2}^*(x, y) \\ &\quad + \tilde{\mathcal{V}}_{T2}^*(x, y) \times \tilde{\mathcal{B}}_{T1}(x, y)], \end{aligned} \quad (11)$$

and where the transverse velocities  $\tilde{\mathcal{V}}_{T2}^{\perp}$  are given in Eq. 7(b). Equation (11) describes the ponderomotive force which couples the plasma beam modes with the em waves.

To fully describe the electron beam we also need to introduce the continuity and Poisson equations:

$$\frac{\partial}{\partial z} \tilde{J}_{zi} = -i\omega_i e \tilde{n}_i, \quad (12)$$

$$\frac{\partial}{\partial z} \tilde{E}_{SC} = -\frac{e}{\epsilon_0} \tilde{n}_i, \quad (13)$$

$$\tilde{J}_{zi} = -e(n_0 \tilde{V}_{zi} + V_{0z} \tilde{n}_i). \quad (14)$$

These equations are written as one-dimensional equations assuming that the  $e$  beam is narrow enough to neglect transverse variations. Three-dimensional effects of the plasma waves can be accounted for but for simplicity will be presently neglected.

Equations (8), (10), and (12)–(14) are now a complete, self-consistent set of equations that need to be solved simultaneously.

### 1. Backward Raman scattering amplifier (conventional FEL)

By substituting  $s$  (signal) for 1 and  $w$  (wiggler) for 2, and making the nondepleted pump approximation,  $C_w = \text{const}$ , we turn (8a) into a linear equation:

$$\frac{dC_s(z)}{dz} = C_w \frac{e}{8 |\mathcal{P}_s|} e^{-i(k_s+k_w)z} \times \tilde{\mathcal{V}}_{Tw}(x_e, y_e) \tilde{n}_i(x_e, y_e, z) \tilde{\mathcal{E}}_{Ts}^*(x_e, y_e) A_e, \quad (15)$$

where  $A_e$  is the effective cross-sectional area of the electron beam, and  $(x_e, y_e)$  are the coordinates of the center of the narrow  $e$  beam.

From Eqs. (10) and (11),

$$\left[ -i\omega_i + V_{0z} \frac{\partial}{\partial z} \right] \tilde{V}_{zi}(z) = -\frac{e}{\gamma_z^2 \gamma_0 m} [\tilde{E}_{SC}(z) + \tilde{E}_{pond}^{\omega_i}(z)], \quad (16)$$

where

$$\tilde{E}_{pond}^{\omega_i} = C_w^* C_s(z) \tilde{\mathcal{E}}_{pond}^{\omega_i} e^{i(k_s+k_w)z},$$

and

$$\begin{aligned} \tilde{\mathcal{E}}_{pond}^{\omega_i} &= \frac{1}{2} (\tilde{\mathcal{V}}_{Ts} \times \tilde{\mathcal{E}}_{Tw}^* + \tilde{\mathcal{V}}_{Tw}^* \times \tilde{\mathcal{E}}_{Ts}), \\ \tilde{\mathcal{V}}_{Tw}^s &= -i \frac{e/(\gamma_0 m)}{\omega_w \mp V_{0z} k_w} [\tilde{\mathcal{E}}_{Tw}^s(x_e, y_e) \\ &\quad + V_{0z} \hat{\mathbf{1}}_z \times \tilde{\mathcal{E}}_{Tw}^s(x_e, y_e)]. \end{aligned} \quad (17)$$

Equations (15), (16), and (12)–(14) are now a set of linear differential equations and can be readily solved by applying the Laplace transform  $\bar{a}(s) = \int_{-\infty}^{\infty} a(z) e^{-sz} dz$ .

Assuming initial conditions  $n_i(0) = V_{zi}(0) = E_{SC}(0) = 0$ , we get for  $\bar{C}_s(s)$  the known gain-dispersion relation of the conventional FEL amplifier:<sup>11</sup>

$$\frac{\bar{C}_s(s)}{C_s(0)} = \frac{(s - i\theta)^2 + \theta_p^2}{s[(s - i\theta)^2 + \theta_p^2] - i\kappa\theta_p^2}, \quad (18)$$

where

$$\theta = \frac{\omega_i}{V_{0z}} - (k_s + k_w) \quad (\text{detuning parameter}),$$

$$\theta_p^2 = \frac{n_0 e^2}{m \gamma_z^2 \gamma_0 \epsilon_0 V_{0z}^2} = \frac{\omega_p'^2}{V_{0z}^2} \quad (\text{space-charge parameter}), \quad (19)$$

$$\kappa = \frac{\epsilon_0}{8 |\mathcal{P}_s|} A_e \tilde{\mathcal{E}}_{Ts}^* \cdot \tilde{\mathcal{V}}_{Tw} |C_w|^2 \tilde{\mathcal{E}}_{pond}^{\omega_i}(k_s + k_w) \quad (\text{coupling parameter}),$$

and where  $\tilde{\mathcal{E}}_{pond}^{\omega_i}$  and the transverse velocities  $\tilde{\mathcal{V}}_{Tw}^s$  are given in Eqs. (16) and (17) and the beat frequency  $\omega_i$  is defined by  $\omega_i = \omega_s - \omega_w$ .

## 2. Backward Raman scattering oscillator

We now analyze the scheme depicted in Fig. 1(b), by substituting for 1 a  $w$  (wiggler) and for 2 an  $s$  (signal). Assuming again an undepleted pump, and following exactly the same analysis of Sec. III A 1 we get a new set of equations:

TABLE I. Summary of the four basic schemes formulation. Use the upper sign of  $k_w$  for the backward scattering schemes and the lower sign for the forward scattering schemes.

	Codirectional interaction amplifiers (convective instability)	Contradirectional interaction oscillators (absolute instability)
$\omega_i$	$\omega_s - \omega_w$	$\omega_w - \omega_s$
$\frac{\bar{C}_s(s)}{C_s(0)}$	$\frac{(s - i\theta)^2 + \theta_p^2}{s[(s - i\theta)^2 + \theta_p^2] - i\kappa\theta_p^2} = \text{gain}$	$\frac{(s + i\theta)^2 + \theta_p^2}{s[(s + i\theta)^2 + \theta_p^2] + i\kappa\theta_p^2} = (\text{gain})^{-1}$
$\theta$	$\frac{\omega_s - \omega_w}{V_{0z}} - (k_s \pm k_w)$	$\frac{\omega_w - \omega_s}{V_{0z}} - (k_s \pm k_w)$
$\kappa$	$\frac{\epsilon_0 A_e}{8  \mathcal{P}_s } \tilde{\mathcal{E}}_{Ts}^* \cdot \tilde{\mathcal{V}}_{Tw} \tilde{\mathcal{E}}_{pond}^{\omega_i}  C_w ^2 (k_s \pm k_w)$	$-\frac{\epsilon_0 A_e}{8  \mathcal{P}_s } \tilde{\mathcal{E}}_{Ts}^* \cdot \tilde{\mathcal{V}}_{Tw} \tilde{\mathcal{E}}_{pond}^{\omega_i}  C_w ^2 (k_s \pm k_w)$
$\tilde{\mathcal{E}}_{pond}^{\omega_i}$	$\frac{1}{2} [\tilde{\mathcal{V}}_{Ts} \times \tilde{\mathcal{E}}_{Tw}^*(x_e, y_e) + \tilde{\mathcal{V}}_{Tw}^* \times \tilde{\mathcal{E}}_{Ts}(x_e, y_e)] \cdot \hat{\mathbf{1}}_z$	$\frac{1}{2} [\tilde{\mathcal{V}}_{Ts}^* \times \tilde{\mathcal{E}}_{Tw}(x_e, y_e) + \tilde{\mathcal{V}}_{Tw} \times \tilde{\mathcal{E}}_{Ts}^*(x_e, y_e)] \cdot \hat{\mathbf{1}}_z$
$\tilde{\mathcal{V}}_{Ts}$	$-i \frac{e/(\gamma_0 m)}{\omega_s - k_s V_{0z}} [\tilde{\mathcal{E}}_{Ts}(x_e, y_e) + V_{0z} \hat{\mathbf{1}}_z \times \tilde{\mathcal{E}}_{Ts}(x_e, y_e)]$	$-i \frac{e/(\gamma_0 m)}{\omega_s + k_s V_{0z}} [\tilde{\mathcal{E}}_{Ts}(x_e, y_e) + V_{0z} \hat{\mathbf{1}}_z \times \tilde{\mathcal{E}}_{Ts}(x_e, y_e)]$
$\tilde{\mathcal{V}}_{Tw}$	$-i \frac{e/(\gamma_0 m)}{\omega_w \pm k_w V_{0z}} [\tilde{\mathcal{E}}_{Tw}(x_e, y_e) + V_{0z} \hat{\mathbf{1}}_z \times \tilde{\mathcal{E}}_{Tw}(x_e, y_e)]$	$-i \frac{e/(\gamma_0 m)}{\omega_w \mp k_w V_{0z}} [\tilde{\mathcal{E}}_{Tw}(x_e, y_e) + V_{0z} \hat{\mathbf{1}}_z \times \tilde{\mathcal{E}}_{Tw}(x_e, y_e)]$
Cubic equation	$(\delta k)^3 - 2\bar{\theta}(\delta k)^2 - (\bar{\theta}_p^2 - \bar{\theta}^2)\delta k + \bar{Q} = 0$	$(\delta k)^3 + 2\bar{\theta}(\delta k)^2 - (\bar{\theta}_p^2 - \bar{\theta}^2)\delta k - \bar{Q} = 0$
$\kappa$	$\frac{1}{4} \frac{A_e}{A_{em}} \frac{\mu e^2}{\gamma_0^2 m^2 c^2}  \hat{\mathbf{l}}_{Ts}^* \cdot \hat{\mathbf{l}}_{Tw} ^2  S_w  \frac{(k_s \pm k_w)^2}{k_s k_w \omega_w}$	
em pump		
$\kappa$	$\frac{1}{4} \frac{A_e}{A_{em}} \frac{e^2}{\gamma_0^2 m^2 c^2}  \hat{\mathbf{b}}_{Ts}^* \cdot \hat{\mathbf{b}}_{Tw} ^2  \bar{B}_{Tw} ^2 \frac{(k_s \pm k_w)^2}{k_s k_w^2}$	
ms pump		

$$\frac{\bar{C}_s(s)}{C_s(0)} = \frac{(s+i\theta)^2 + \theta_p^2}{s[(s+i\theta)^2 + \theta_p^2] + i\kappa\theta_p^2}, \quad (20)$$

where

$$\begin{aligned} \theta &= \frac{\omega_i}{V_{0z}} - (k_s + k_w) \quad (\omega_i = \omega_w - \omega_s), \\ \theta_p^2 &= \frac{e^2 n_0}{m \gamma_z^2 \gamma_0 \epsilon_0 V_{0z}^2} = \frac{\omega_p'^2}{V_{0z}^2}, \\ \kappa &= -\frac{\epsilon_0}{8 |\mathcal{P}_s|} A_e \tilde{\mathcal{E}}_{Ts}^* \cdot \tilde{\mathcal{V}}_{Tw} |C_w|^2 \tilde{\mathcal{E}}_{\text{pond}}^{\omega_i}(k_s + k_w), \\ \tilde{E}_{\text{pond}}^{\omega_i} &= C_w \tilde{C}_s^*(z) \tilde{\mathcal{E}}_{\text{pond}}^{\omega_i} e^{i(k_s + k_w)z}, \\ \tilde{\mathcal{E}}_{\text{pond}}^{\omega_i} &= \frac{1}{2} (\tilde{\mathcal{V}}_{Ts} \times \tilde{\mathcal{B}}_{Tw}^* + \tilde{\mathcal{V}}_{Tw}^* \times \tilde{\mathcal{B}}_{Ts}), \\ \tilde{\mathcal{V}}_{Ts}^w &= -i \frac{e/(\gamma_0 m)}{\omega_s^w + V_{0z} k_s} (\tilde{\mathcal{E}}_{Ts}^w + \tilde{V}_{0z} \hat{1}_z \times \tilde{\mathcal{B}}_{Ts}^w). \end{aligned} \quad (21)$$

Excepting  $\omega_i$ ,  $\theta$ , and  $\tilde{\mathcal{V}}_T$ , these equations are identical with the gain-dispersion relation of the conventional FEL [Fig. 1(a)] but is applied here for the backward-propagating signal-wave scheme (1b). Nevertheless, there is an important difference between the two sets of equations: In the conventional FEL scheme, where the signal is propagating from left to right in the  $+z$  direction, the expression for  $\bar{C}_s(s)/C_s(0)$  is the gain-dispersion function (the signal wave enters the interaction region at  $z=0$  and its output value is evaluated at  $z=L$ ), while in the backward Raman scattering oscillator, where the signal enters the interaction region at  $z=L$  and couples out at  $z=0$ , the expression  $\bar{C}_s(s)/C_s(0)$  represents  $(\text{gain})^{-1}$ . Thus the inverse Laplace transform of Eq. (20) is  $(\text{gain})^{-1}$  as a function of the interaction length.

The gain-dispersion relations of the backward Raman scattering amplifier and oscillator and the associated parameters definitions are summarized in Table I in a comparative way. Use the upper sign of  $k_w$  for the backward Raman scattering schemes.

### B. Forward Raman scattering schemes

The generalization of our analysis to the forward Raman scattering schemes [represented by Figs. 1(c) and 1(d)] is straightforward. From the point of view of signal-idler-wave interaction in the nondepleted pump regime there is no substantial difference between the codirectional interaction amplifiers with backward Raman scattering [Fig. 1(a)] or forward Raman scattering [Fig. 1(d)], and the same can be said on the backward [Fig. 1(b)] and forward [Fig. 1(c)] Raman scattering contradirectional interaction oscillations. Consequently, the gain-dispersion relations of the forward Raman scattering amplifier and oscillator can be derived by substituting  $k_w \rightarrow -k_w$  in all the derivation steps of the backward Raman scattering amplifier (Sec. III A 1) and oscillator (Sec. III A 2), respectively. We thus obtain the following expressions for the forward Raman scattering amplifier:

$$E_w^s = \text{Re}[C_w^s(z) \tilde{\mathcal{E}}_w^s(x, y) e^{ik_w^s z - i\omega_w^s t}], \quad (22)$$

$$B_w^s = \text{Re}[C_w^s(z) \tilde{\mathcal{B}}_w^s(x, y) e^{ik_w^s z - i\omega_w^s t}],$$

$$\omega_i = \omega_s - \omega_w,$$

(23)

$$E_{\text{pond}}^{\omega_i} = \text{Re}[C_s(z) C_w^* \tilde{\mathcal{E}}_{\text{pond}}^{\omega_i} e^{i(k_s - k_w)z - i\omega_i t}].$$

For the forward Raman scattering oscillator,

$$E_w^s = \text{Re}[C_w^s(z) \tilde{\mathcal{E}}_w^s(x, y) e^{-ik_w^s z - i\omega_w^s t}], \quad (24)$$

$$B_w^s = \text{Re}[C_w^s(z) \tilde{\mathcal{B}}_w^s(x, y) e^{-ik_w^s z - i\omega_w^s t}],$$

$$\omega_i = \omega_w - \omega_s,$$

(25)

$$E_{\text{pond}}^{\omega_i} = \text{Re}[C_s^*(z) C_w \tilde{\mathcal{E}}_{\text{pond}}^{\omega_i} e^{i(k_s - k_w)z - i\omega_i t}].$$

The analogous derivation steps lead eventually to the same gain-dispersion relations and associated parameters definitions derived before for the backward Raman scattering instabilities with the transformation  $k_w \rightarrow -k_w$ . These expressions are summarized in Table I in which the lower sign of  $k_w$  corresponds to the forward scattering schemes.

We note that in all cases  $\omega_i$  may be positive or negative without loss of the generality of the derivation. The different definitions of  $\omega_i$  for the amplifier and oscillator cases were chosen to keep  $\omega_i$  positive in the most common configurations of the backward Raman scattering schemes.

## IV. NUMERICAL RESULTS AND ASYMPTOTIC DISPERSION RELATIONS

In the previous section we derived the four basic scattering schemes in such a way that they differ from each other in the final equations only by changes of signs of  $k_w$  and in the detuning parameter.

From the second row of Table I we see that the dispersion functions  $\bar{C}_s(s)/C_s(0)$  are independent of the sign of  $k_w$  and therefore are the same for the backward and forward scattering schemes. Furthermore, the two expressions of the dispersion equations may be written by a single formula:

$$\frac{\bar{C}_s(s)}{C_s(0)} = \frac{(s \pm i\theta)^2 + \theta_p^2}{s[(s \pm i\theta)^2 + \theta_p^2] \pm i\kappa\theta_p^2}, \quad (26)$$

where the plus sign is used for the amplifiers [convective instabilities, Figs. 1(a) and 1(d)] and the minus sign is used for the oscillators [absolute instabilities, Figs. 1(b) and 1(c)].

Inverse transforming Eq. (26), and evaluating  $C_s(z)/C_s(0)$  at  $z=L$  where  $L$  is the interaction length, yields the same equation for all four schemes:

$$\frac{C_s(L)}{C_s(0)} = \frac{\mp \bar{Q}}{(\delta k_1 - \delta k_2)(\delta k_1 - \delta k_3)(\delta k_2 - \delta k_3)} \times \left[ \frac{\delta k_2 - \delta k_3}{\delta k_1} e^{i\delta k_1} + \frac{\delta k_3 - \delta k_1}{\delta k_2} e^{i\delta k_2} + \frac{\delta k_1 - \delta k_2}{\delta k_3} e^{i\delta k_3} \right], \quad (27)$$

where  $\delta k_i$  ( $i=1,2,3$ ) are the roots of one of the cubic equations

$$(\delta k)^3 + 2\bar{\theta}(\delta k)^2 - (\bar{\theta}_p^2 - \bar{\theta}^2)\delta k - \bar{Q} = 0, \quad (28)$$

for oscillators [Figs. 1(b) and 1(c)] or

$$(\delta k)^3 - 2\bar{\theta}(\delta k)^2 - (\bar{\theta}_p^2 - \bar{\theta}^2)\delta k + \bar{Q} = 0, \quad (29)$$

for amplifiers [Figs. 1(a) and 1(d)], and for both cases

$$\begin{aligned} \bar{\theta} &= \bar{\theta}L, \\ \bar{\theta}_p &= \theta_p L, \\ \bar{Q} &= \kappa \bar{\theta}_p^2 L. \end{aligned} \quad (30)$$

The coupling parameter  $\kappa$  was calculated explicitly for arbitrarily polarized transverse electromagnetic and magnetostatic pumps (in the latter case  $\omega_w = 0$ ). The results are summarized in the last two rows of Table I.  $\hat{\mathbf{i}}_{T_w}^s = \tilde{\mathcal{E}}_{T_w}^s / |\tilde{\mathcal{E}}_{T_w}^s|$  and  $\hat{\mathbf{b}}_{T_w}^s = \tilde{\mathcal{B}}_{T_w}^s / |\tilde{\mathcal{B}}_{T_w}^s|$  are the polarization (complex) unit vectors of the electric and magnetic fields, respectively.  $A_{em}$  is an effective cross-section area of the signal wave, defined by  $\frac{1}{2} \text{Re}[\tilde{\mathcal{E}}_s(x_e, y_e) \times \tilde{\mathcal{H}}_s^*(x_e, y_e)] \cdot \hat{\mathbf{i}}_z A_{em} = \mathcal{P}_s$  where  $\mathcal{P}_s$  is

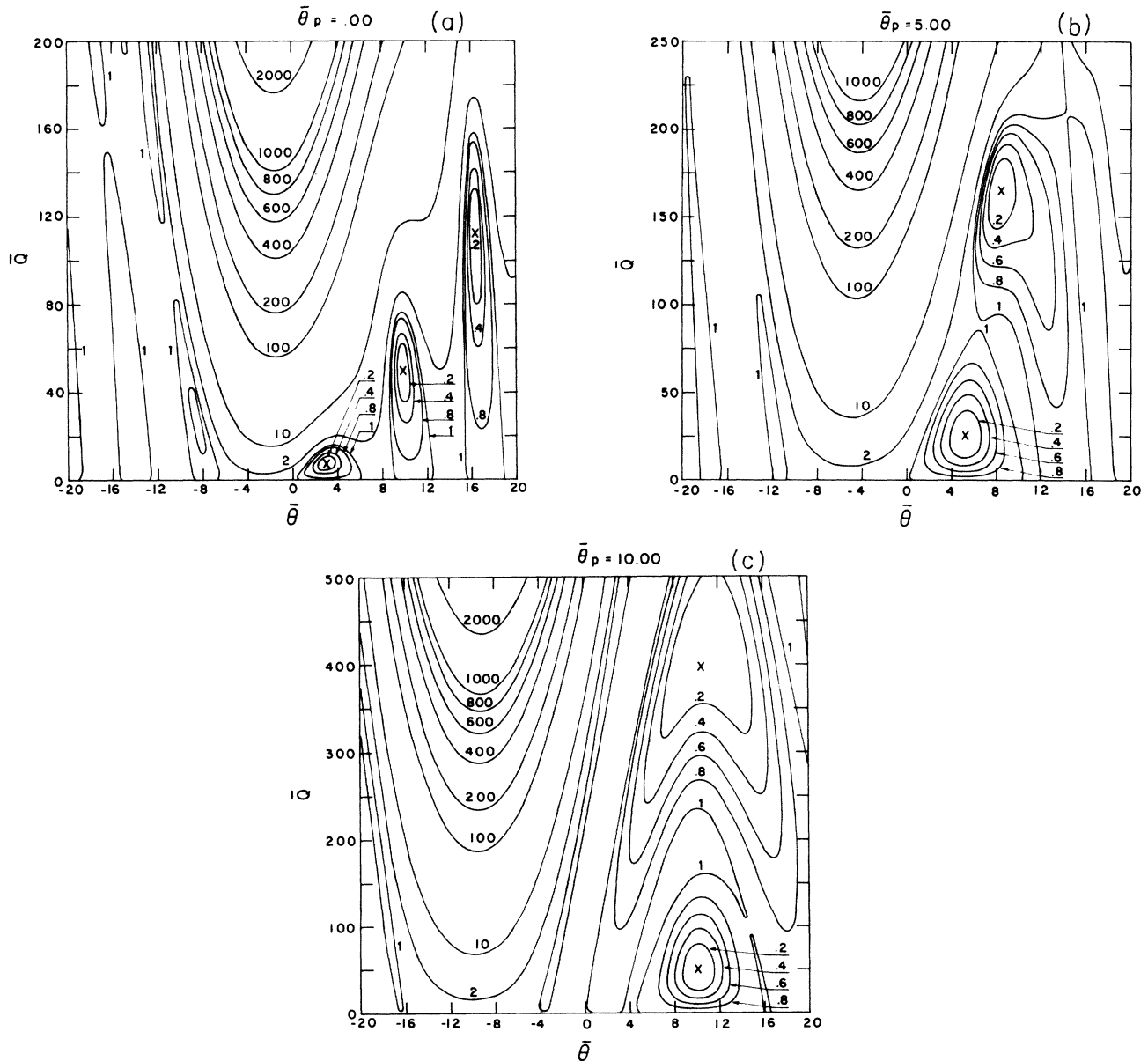


FIG. 4. Contour maps of  $|C_s(L)/C_s(0)|^2$  for three values of  $\bar{\theta}_p$ . (a)  $\bar{\theta}_p = 0$ , (b)  $\bar{\theta}_p = 5$ , (c)  $\bar{\theta}_p = 10$ . The oscillation points are marked by  $\times$ .

the mode normalization power [Eq. (3)] and  $(x_e, y_e)$  are the  $e$ -beam center coordinates.  $S_w$  is the average power density carried by the wiggler field in the electromagnetic pump case, and  $\bar{B}_w$  is the rms value of the wiggler strength in the magnetostatic pump case. Note that for all cases the calculated value of  $\kappa$  is always positive. Also note that the maximum coupling coefficient is obtained when the wiggler and signal waves have the same polarization, and this maximum value is the same for linear or circular (helical) polarization. (The comparison of different polarizations should be done with wigglers of the same average power density or rms magnetic field.)

Equations (28) and (29) are third-order algebraic equations which have explicit solutions for  $\delta k_i$  ( $i=1,2,3$ ).<sup>14</sup> The only difference between the two equations is in the sign of the second and fourth coefficients. This difference causes only a change of sign in all three roots but does not change their absolute value.<sup>14</sup> It is straightforward to show that changing the sign of all three roots leaves the absolute value of  $C_s(L)/C_s(0)$  [Eq. (27)] unchanged (see Appendix B). This result enables us to use a single formula to describe all four cases.

The explicit analytic expressions for the roots of (28) (Ref. 14) were substituted in (27) and the amplitude ratio  $C_s(L)/C_s(0)$  was computed numerically. The power-gain parameter  $|C_s(L)/C_s(0)|^2$  is displayed in Fig. 4 in a contour map in the  $\bar{\theta}$ - $\bar{Q}$  plane with  $\bar{\theta}_p$  as a parameter. [The contours are for constant value of  $|C_s(L)/C_s(0)|^2$ ]. The maps can be used for all the four scattering schemes depicted in Fig. 1, with the help of Eqs. (30) where the corresponding definitions of  $\theta$  and  $\kappa$  for each scattering scheme are given in Table I.

As already mentioned, Eq. (27) is the small-signal gain function for the right-going signal schemes [amplifiers, Figs. 1(a) and 1(d)] and the small-signal (gain)<sup>-1</sup> for the left-going signal schemes [oscillators, Figs. 1(b) and 1(c)]. Thus, when  $|C_s(L)/C_s(0)|^2=0$ , the linear gain for the left-going waves goes to infinity, and oscillations (absolute instability) are excited in the beam. Three oscillation points are clearly identified in the first quadrant of the  $(\bar{Q}, \bar{\theta})$  plane ( $\bar{Q}, \bar{\theta} > 0$ ) in Fig. 4(a) ( $\bar{\theta}_p=0$ ). In Figs. 4(b) and 4(c) ( $\bar{\theta}_p=5, 10$ ) two oscillation points (modes) are identified within the parameters region shown. The value of  $|C_s(L)/C_s(0)|^2$  was checked to be less than  $10^{-10}$  at these oscillation points.

When one changes the space-charge parameter  $\bar{\theta}_p$ , the oscillation points coordinates move in the  $\bar{\theta}, \bar{Q}$  plane. This movement was analyzed numerically for the first two oscillation orders and the dependences of the oscillation points  $(\bar{Q}, \bar{\theta})$  values on  $\bar{\theta}_p$  are shown in Figs. 5(a) and 5(b) for the first oscillation mode order, and in Figs. 6(a) and 6(b) for the second oscillation order.

Let us examine now the asymptotic behavior of the detuning parameter  $\bar{\theta}$  at the oscillation points. It is evident from Fig. 5(b) that for  $\bar{\theta}_p \gg 1$  oscillation always takes place at  $\bar{\theta} \simeq \bar{\theta}_p$ . Using the definitions of  $\bar{\theta}$  for both kinds of oscillators (Table I) one finds the asymptotic relation

$$\frac{\omega_i}{V_{0z}} - k_i = \theta_p = \frac{\omega_p'}{V_{0z}}, \quad (31)$$

where  $\omega_p'$  is the longitudinal plasma frequency.  $\omega_i$  is the

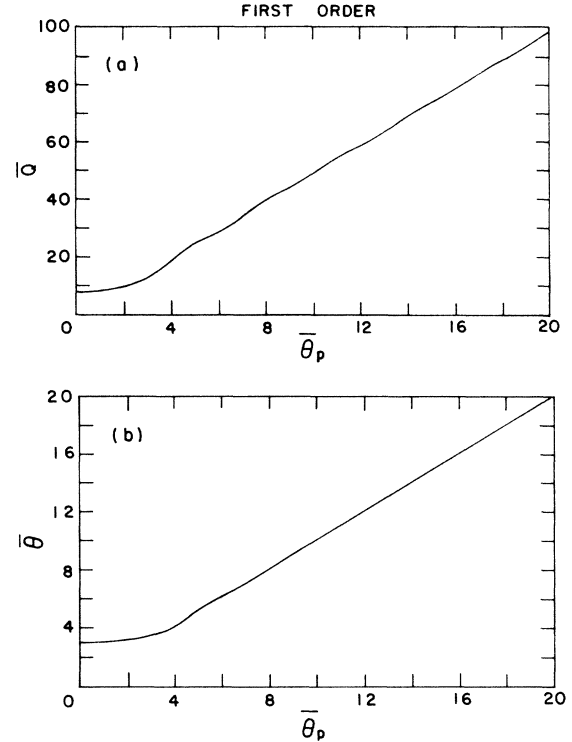


FIG. 5. Parameters of the oscillation conditions for the first-order oscillation. (a) Gain parameter  $\bar{Q}$  vs  $\bar{\theta}_p$  and (b) detuning parameter  $\bar{\theta}$  vs  $\bar{\theta}_p$ . Note the asymptotic linear behavior of  $\bar{\theta}$  for large values of  $\bar{\theta}_p$ .

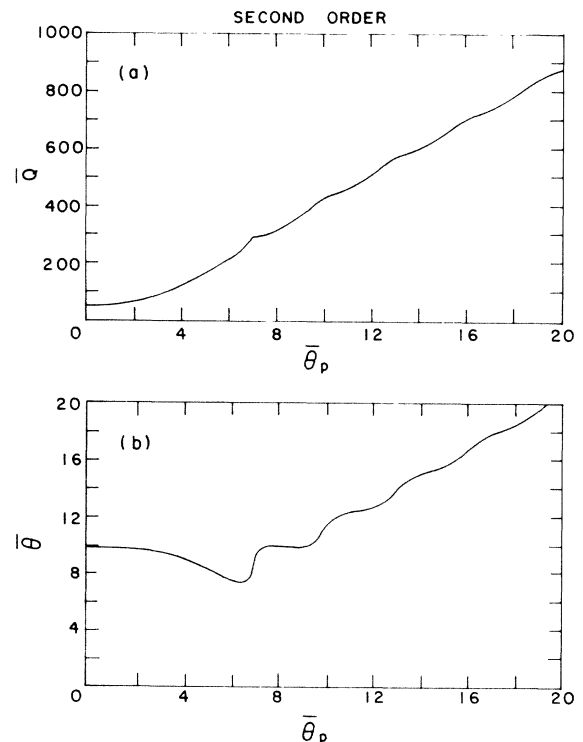


FIG. 6. Parameters of the second-order oscillation condition.

beat frequency which is defined for the oscillators (contra-directional interaction) schemes as  $\omega_i = \omega_w - \omega_s$  (see Table I);  $k_i = k_s + k_w$  for the backward Raman scattering oscillator and  $k_i = k_s - k_w$  for the forward Raman scattering oscillator.

$\omega_i$  and  $k_i$  are the frequency and wave number of the ponderomotive force which by modulating the beam excites the idler wave ( $\omega_i, k_i$ ). The dispersion relations of the space-charge waves are as follows. The fast-wave relations are

$$\omega = \begin{cases} V_{0z}k + \omega'_p, & \omega > 0 \\ V_{0z}k - \omega'_p, & \omega < 0. \end{cases} \quad (32)$$

The slow-wave relations are

$$\omega = \begin{cases} V_{0z}k - \omega'_p, & \omega > 0 \\ V_{0z}k + \omega'_p, & \omega < 0. \end{cases} \quad (33)$$

Comparison of Eqs. (32) and (33) with (31) confirms right away our assertion that the oscillators involve coupling to the fast space-charge wave when  $\omega_i = \omega_w - \omega_s > 0$  (down conversion<sup>5</sup>) and to the slow space-charge wave when  $\omega_i = \omega_w - \omega_s < 0$  (up conversion<sup>1</sup>).

In a similar way it is possible to show that the amplifier (convective instability) schemes acquire in the asymptotic limit  $\bar{\theta}_p \gg 1$  maximum gain at  $\bar{\theta} = -\bar{\theta}_p$  [inspect Figs. 4(b) and 4(c)]. Since in these schemes we defined  $\omega_i = \omega_s - \omega_w$  (Table I) we conclude that the amplification process involves coupling to the slow space-charge wave in the up-conversion amplifiers which are shown in Fig. 2(a) (and as well known for the conventional FEL amplifier) and to the fast space-charge wave in the peculiar down-conversion amplifiers like the one shown in Fig. 2(d).

## V. THRESHOLD CONDITIONS

In this section we derive an asymptotic threshold condition expression for all kinds of oscillations in the limit  $\bar{\theta}_p \gg 1$ , and compare it to the numerical results. We start with the oscillator's dispersion relation (20):

$$\frac{\bar{C}_s(s)}{C_s(0)} = \frac{(s + i\theta)^2 + \theta_p^2}{s[(s + i\theta)^2 + \theta_p^2] + i\kappa\theta_p^2}.$$

Following the arguments of the last section, we assume  $\theta \simeq \theta_p$ , and obtain

$$\frac{\bar{C}_s(s)}{C_s(0)} \Big|_{\theta=\theta_p} = \frac{s(s + 2i\theta_p)}{s^2(s + 2i\theta_p) + i\kappa\theta_p^2}. \quad (34)$$

Making now the small growth rate assumption  $|s| \ll 2\theta_p$  (Ref. 5) one finds

$$\frac{\bar{C}_s(s)}{C_s(0)} = \frac{s}{s^2 + \frac{1}{2}\kappa\theta_p}. \quad (35)$$

Inverse transforming Eq. (35), evaluating  $C_s(z)/C_s(0)$  at  $z=L$  we find

$$\frac{C_s(L)}{C_s(0)} = \cos\left[\left(\frac{1}{2}\kappa\theta_p\right)^{1/2}L\right],$$

which yields, for the oscillation condition  $[C_s(L)/$

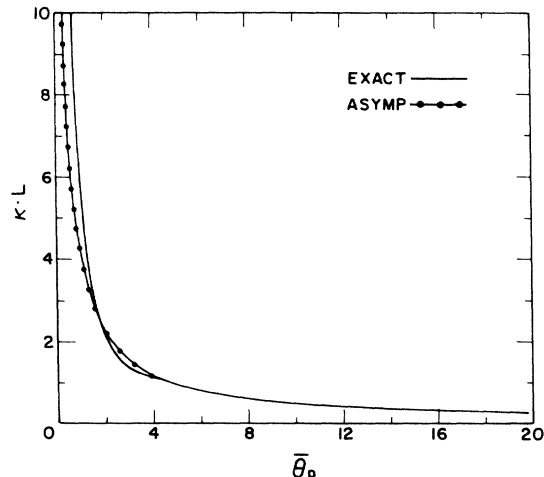


FIG. 7. Plot of  $\kappa L$  vs  $\bar{\theta}_p$  for the first-order oscillation. The asymptotic expression is in agreement with the exact numerical results for  $\bar{\theta}_p > 4$ .

$C_s(0)=0]$ ,

$$L = \pi(1 + 2n) \frac{1}{\sqrt{2\kappa\theta_p}}, \quad (36)$$

or, for the lowest oscillation order ( $n=0$ ),

$$L_{\min} = \frac{\pi}{\sqrt{2\kappa\theta_p}}. \quad (37)$$

Equation (37) is a general expression for the oscillation threshold, and can be used for electromagnetically or statically pumped devices, and for any kind of the pump polarization by using the corresponding definitions of  $\kappa$  which are given in the previous sections and in Table I. The asymptotic approximation [Eq. (37)]  $\kappa L = \pi^2/2\theta_p L$  is drawn together with the numerically computed threshold condition in Fig. 7. The figure displays excellent agreement between the curves for  $\bar{\theta}_p \geq 4$ .

## VI. SOME SPECIFIC FEL SYSTEMS

We turn now to calculate explicit expressions for the oscillation conditions of two common absolute instability examples.

### A. Backward Raman scattering oscillator with an em pump

This instability is the one proposed in Ref. 5. The expression for  $\kappa$  as given in Table I is

$$\kappa = \frac{1}{4} \frac{A_e}{A_{em}} \frac{\mu e^2}{\gamma_0^2 m^2 c^2} |\hat{I}_{rs}^* \cdot \hat{I}_{tw}|^2 |S_w| \frac{(k_s + k_w)^2}{k_s k_w \omega_w}. \quad (38)$$

Assuming that the em dispersion relation is approximately  $\omega_{sw} = c k_{sw} \gg \omega'_p$ , and  $\theta \simeq \theta_p$ , we get an expression for  $\omega_s$ :

$$\omega_s = \frac{\omega_w(1 - \beta_z) + \omega_p}{1 + \beta_z} \simeq \omega_w \frac{1 - \beta_z}{1 + \beta_z}, \quad (39)$$

where  $\beta_z = V_{0z}/c$ . Substituting (39) in (38), and assuming

$|\hat{\mathbf{T}}_{Ts}^* \cdot \hat{\mathbf{T}}_{Tw}| = 1$ , we find

$$\kappa \cong \frac{\mu e^2}{m^2 c^2 \omega_w} \frac{A_e}{A_{em}} |S_w| \left[ \frac{\gamma_z}{\gamma_0} \right]^2 \quad (40)$$

which, together with (37), yields

$$L_{\min} = \pi \frac{mc}{e} \left[ \frac{\omega_w V_{0z} \gamma_z \gamma_0^{1/2}}{2\mu\omega_p |S_w|} \frac{A_{em}}{A_e} \right]^{1/2} (1 + \bar{a}_w^2)^{1/2}. \quad (41)$$

Equation (41) determines the threshold value of the interaction length for a given pump strength. Note that this equation is not valid in the tenuous beam limit.

### B. Forward Raman scattering oscillator, with a transverse magnetostatic linear or helical wiggler

This kind of instability is the absolute instability analyzed before in Refs. 1–4. We follow now the same procedure of the first example. Assuming the dispersion relation of the signal wave is approximately  $\omega_s \simeq ck_s \gg \omega'_p$ , we get an expression for  $k_s$ :  $k_s \simeq k_w \beta_z / (1 + \beta_z)$ . Using the appropriate expression for  $\kappa$  given in Table I,

$$\kappa = \frac{1}{4} \frac{A_e}{A_{em}} \frac{e^2}{\gamma_0^2 m^2 c^2} |\hat{\mathbf{b}}_{Ts}^* \cdot \hat{\mathbf{b}}_{Tw}|^2 |\bar{B}_{Tw}|^2 \frac{(k_s - k_w)^2}{k_s k_w^2}, \quad (42)$$

assuming  $|\hat{\mathbf{b}}_{Ts}^* \cdot \hat{\mathbf{b}}_{Tw}| = 1$  and inserting  $k_s$ , we find

$$\kappa = \frac{1}{4} \frac{A_e}{A_{em}} \frac{e^2}{\gamma_0^2 m^2 c^2} |\bar{B}_{Tw}|^2 \frac{1}{k_w \beta_z (1 + \beta_z)}, \quad (43)$$

where  $\beta_z = V_{0z}/c$ . Substituting (43) into (37) we get a final expression for the threshold length:

$$L_{\min} = \frac{\pi c}{\omega_c} \gamma_0^{5/4} \left[ 2 \frac{k_w V_{0z} \beta_z (1 + \beta_z) \gamma_z}{\omega_p} \frac{A_{em}}{A_e} \right]^{1/2}, \quad (44)$$

where  $\omega_c = e |\bar{B}_{Tw}| / m$  in MKS units.

This absolute instability was investigated theoretically and numerically by Liewer *et al.*<sup>1</sup> for the special case of a helical wiggler. It is possible to compare both results in the limiting case of a highly relativistic beam (which was assumed in Liewer's analysis). In this case we get

$$L_{\min} = \frac{2\pi c \gamma_0^{5/4} \gamma_z^{1/2}}{\omega_c} \left[ \frac{ck_w}{\omega_p} \frac{A_{em}}{A_e} \right]^{1/2} \quad (45)$$

which differs from Liewer's results only by the introduction of the filling factor  $A_e/A_{em}$  and the  $\gamma$  correction  $\gamma_z^2 = \gamma_0^2 / (1 + \bar{a}_w^2)$ .

It is important to notice that in Liewer's analysis there is a hidden assumption of interaction with the slow plasma wave only. This corresponds to the limiting case  $\bar{\theta}_p \gg 1$ , which is also the validity condition of our analytical expression (45). However, our analysis is valid beyond this limit, for arbitrary values of  $\bar{\theta}_p$  including the tenuous beam limit,  $\bar{\theta}_p < 1$ , but one must then use the numerically computed curves of Fig. 5 in order to evaluate the oscillation threshold.

In the conclusion of this work, we examine the thresh-

old conditions for excitation of various absolute instabilities in a conventional magnetostatically pumped FEL. Consider, as shown in Fig. 8, a helical or linear magnetostatic wiggler FEL system which amplifies a short-wavelength em signal  $S_1$  propagating from left to right. Two kinds of instability can exist: the first one is the magnetostatically pumped slow space-charge wave instability,<sup>1</sup> the second is the em-pumped fast space-charge wave instability, in which  $S_1$  acts as an em wiggler field. In both cases the excited signal is a long-wavelength em field  $S_2$  which propagates from right to left.

The radiation condition of  $S_1$  is well known:  $\omega_{S_1} = ck_w 2\gamma_z^2$  where  $\omega_{S_1}$  is the radian frequency of  $S_1$ ,  $k_w = 2\pi/\lambda_w$ ,  $\lambda_w$  is the static wiggler period and  $\gamma_z^2 = \gamma_0^2 / (1 + \bar{a}_{WMS}^2)$ , with  $\bar{a}_{WMS}$  defined as  $\bar{a}_{WMS} = e\bar{B}_w / mck_w$  ( $\bar{B}_w$  is the wiggler rms magnetic field strength). The radiation condition for  $S_2$  involves two different calculations, which lead to the same results: for the magnetostatically pumped instability we set  $\theta = -\omega_{S_2}/V_{0z} - (k_{S_2} - k_w) = 0$  which leads to the condition  $\omega_{S_2} = \frac{1}{2}ck_w$ . Similarly, for the em-pumped instability we set  $\theta = (\omega_{S_1} - \omega_{S_2})/V_{0z} - (k_{S_2} + k_{S_1}) = 0$  which, upon substituting the radiation condition of  $\omega_{S_1}$  leads again to the relation  $\omega_{S_2} = \frac{1}{2}ck_w$ .

Inserting  $\omega_{S_1}$  as  $\omega_w$  in Eq. (41), and defining a "threshold-ratio" parameter as the ratio between  $L_{\min}^{ms}$  and  $L_{\min}^{em}$  (which are the threshold lengths of the magnetostatically pumped and electromagnetically pumped instabilities, respectively), we find, after taking the limit  $\gamma \gg 1$

$$\mathcal{R} = \frac{L_{\min}^{ms}}{L_{\min}^{em}} = \left[ \frac{|S_{em}|}{\frac{1}{4} \sqrt{\epsilon_0/\mu c^2} |\bar{B}_{Tw}|^2} \right]^{1/2}, \quad (46)$$

where  $S_{em}$  is the average power density of the electromagnetic signal  $S_1$ . Equation (46) determines what instability is more dominant for a given FEL system, designed to operate at a given wiggler strength and to produce a given signal power. If  $\mathcal{R} > 1$  one must check the stability criteria of the electromagnetically pumped oscillations using Eq. (41), if  $\mathcal{R} < 1$  then the magnetostatically pumped instability is dominant and Eq. (44) is the relevant stability criteria.

We now calculate two specific numerical examples using typical parameters occurring in high-power FEL designs.<sup>15</sup> Consider a FEL system with the following parameters:  $\lambda_w = 10$  cm ( $\omega_w = 0$ ),  $\gamma_0 = 9$ ,  $\bar{B}_w = 3$  kG,  $J_0 = 50$  A/cm<sup>2</sup>,  $A_{em}/A_e = 25$ , and the circulating em power densi-

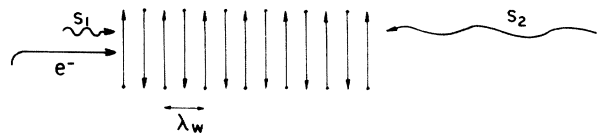


FIG. 8. Conventional, magnetostatically pumped FEL amplifier.  $S_1$  is the amplified signal and  $S_2$  is an em wave excited by the instability of the beam. This instability can be pumped by the static wiggler (slow-wave instability) or by the em signal  $S_1$  (fast-wave instability).

ty of  $S_1$  is about 96 MW/cm<sup>2</sup>. Using Eq. (46) we find  $\mathcal{R}=0.42$ , thus the dominant instability is the magnetostatically pumped one. Using (45) we get

$$L_{\min}=8.7 \text{ m} .$$

Thus the instability will be excited if the interaction length  $L$  is greater than 8.7 m. Now we turn to check the validity of our calculations: the above parameters correspond to  $\omega_p=5.8 \times 10^9 \text{ sec}^{-1}$  which yields  $\theta_p=2.1 \text{ m}^{-1}$  ( $\theta_p=\omega_p/\gamma_z \gamma_0^{1/2} V_{0z}$ ) thus  $\bar{\theta}_p=18.6$ , and our result is, according to Fig. 7, in good agreement with the numerical calculations.

For the second example we multiply the current density  $J_0$  of the first example by 10, which leads to  $J_0=500 \text{ A/cm}^2$  and to a circulating power density about 1 GW/cm<sup>2</sup> (the saturation power is proportional to current density<sup>11</sup>), all the other parameters are the same as those of the first example. The instability ratio for this system is about 1.36, thus the electromagnetically pumped instability is dominant, using Eq. (41) we find the threshold length to be about 3.6 m. These parameters correspond to  $\omega_p=1.8 \times 10^{10} \text{ rad/sec}$ , which together with  $L=3.6 \text{ m}$  leads to  $\bar{\theta}_p=24$  ( $\bar{\theta}_p=\omega_p L/\gamma_z \gamma_0^{1/2} V_{0z}$ ), and again our asymptotic calculations are valid.

In conclusion, two short comments regarding the stability of a general FEL system are in order.

(a) In the last section only two absolute instability schemes were computed and compared, but it is important to notice that in a general FEL system (especially oscillators with optical resonators) other instabilities like the em-pumped forward Raman scattering oscillator and amplifier depicted in Figs. 1(c) and 1(d), respectively, can give rise to oscillation, due to the high-intensity circulating fields in the cavity. All possible parasitic instability processes should be evaluated in specific high-power FEL laser designs.

(b) In the stability analysis of the present paper we assumed a stationary time dependence  $\exp(i\omega t)$  and a continuous electron beam. Infinite-gain conditions were interpreted as absolute instabilities, which would tend to amplify the noise in the system up to saturation. Some relevant questions about the oscillation buildup time and stability criterions of finite-pulse FEL devices are still left open. In particular if the parasitic oscillations buildup times are long relative to the FEL pulse duration, the effect of the parasitic oscillation in the FEL operation may not be of significant concern.

#### ACKNOWLEDGMENT

This research was supported in part by the U.S. Air Force Office of Scientific Research, Department of the Air Force, under Grant No. AFOSR-82-0239.

#### APPENDIX A

We discuss now the various interaction schemes following Fig. 1. Figure 1(a) corresponds to the conventional FEL amplifier (convective instability), in which the wiggler wave propagates in counter direction to the electron beam and the signal wave. The Stokes diagrams of

this interaction scheme in the collective limit  $\bar{\theta}_p \gg 1$  are represented by the left-going vectors of Fig. 2(a). The Stokes diagrams express the conservation of energy and momentum conditions in the three-wave parametric coupling process involving the pump (wiggler) wave  $(0, -k_w)$  or  $(\omega_w, -k_w)$  (corresponding to static and electromagnetic pumps, respectively), the signal wave  $(\omega_s, k_s)$ , and the idler wave  $(\omega_i, k_i)$ , which in this case is the slow space-charge wave. The three-waves interaction is strong when the phase matching conditions  $\omega_i=\omega_s-\omega_w$  and  $k_i=k_s+k_w$  are satisfied. Alternatively, the condition of strong interaction can be expressed in terms of a synchronism condition between the phase velocities of the ponderomotive wave and the idler (slow space-charge) waves  $V_{\text{pm}}=V_{\text{sc}}$ .<sup>11</sup> The ponderomotive wave is the force field produced by the beating of the two electromagnetic waves via the nonlinear Lorentz force equation and it propagates with phase velocity  $V_{\text{pm}}=(\omega_s-\omega_w)/(k_s+k_w)$ . The phase velocity of the slow space-charge wave is  $V_{\text{sl}}=V_{0z}/(1+\omega_p'/|\omega_i|)$ . The phase matching and the synchronism conditions are, of course, equivalent.

In Fig. 1(b) the roles of the pump and signal waves were interchanged. The signal wave propagates in counter direction to the beam and pump wave. Since the interacting signal wave and electron beam propagate in counter directions, a feedback mechanism is constituted, and contradirectional interaction oscillation (absolute instability) may be excited. This is the instability that was analyzed in Ref. 5, and we have shown that in the case of down (up) conversion it involves excitation of the fast (slow) plasma wave of the beam. The right-going vector of Fig. 2(b) shows the Stokes diagram of this scattering scheme. It is seen that the fast plasma wave  $(-\omega_i, -k_i)=(\omega_s-\omega_w, -k_s-k_w)$  can be coupled to the down-converted signal wave  $(\omega_s, -k_s)$  via the right-going wave  $(\omega_w, k_w)$  where  $\omega_s < \omega_w$ .

In Fig. 1(c) the scattered wave propagates in the same direction as the pump wave, and both of them opposite to the beam. If coupling to the electron-beam space-charge waves is possible then evidently this scheme constitutes again a contradirectional interaction feedback mechanism between the signal and the beam waves, and consequently oscillation (absolute instability) may be excited.

It is somewhat difficult at first glance to become convinced that synchronization between the ponderomotive force and any of the plasma waves is possible in the scheme 1(c), because one normally would expect the space-charge waves to propagate in the right direction with speed close to the beam velocity and the ponderomotive wave to propagate in this scheme leftward. Closer examination shows that both of these assumptions are not always true. The phase velocity of the fast space-charge wave is  $V_f=V_{0z}/(1-\omega_p'/|\omega_i|)$  and when  $|\omega_i|=|\omega_s-\omega_w| < \omega_p'$ , then  $v_f < 0$  and the fast space-charge wave propagates in counter direction to the electron beam. In this case the fast space-charge wave may couple to a left-going ponderomotive wave produced by two left-going normal electromagnetic waves. The Stokes diagram of this scheme is represented by the left-going vector in Fig. 2(b). Apart from the wiggler direction, the interaction scheme is basically the same fast-wave oscilla-

tion of Fig. 1(b).

Another way by which the forward scattering scheme of Fig. 1(c) may be realized, is by synchronizing the right-going slow space-charge wave of phase velocity  $V_{sl} = V_{0z} / (1 + \omega_p' / |\omega_i|)$  to a right-going ponderomotive wave. The phase velocity of the ponderomotive wave generated by two left-going electromagnetic waves is  $V_{pm} = -(\omega_s - \omega_w) / (k_s - k_w)$  and with any normal electromagnetic modes (free-space or uniform waveguide modes) it is negative. However, if  $(\omega_w, -k_w)$  is allowed to be a slow electromagnetic wave:  $\omega_w / k_w < c$  (e.g., a slow space harmonic of a Floquet mode in a periodic waveguide<sup>6</sup>) or simply a static wiggler:  $\omega_w = 0$ , then it is possible to obtain  $k_s < k_w$  and consequently  $V_{pm} > 0$ . The synchronization with the slow space-charge wave is then possible. The Stokes diagram of this case is shown in Fig. 2(c) for both slow electromagnetic and static pumps. The static pump case is the instability that was analyzed in Ref. 1.

In Fig. 1(d) an interesting new scheme of forward Raman scattering FEL amplifier is shown. In this case both signal and wiggler waves propagate in the same direction with the electron beam. Such forward Raman scattering amplification (convective instability) schemes can take place with both up and down conversion involving coupling to the slow and fast space-charge waves, respectively. The Stokes diagram of the forward Raman scattering slow space-charge wave instability is represented by the right-going vector in Fig. 2(a) and the fast space-charge wave instability is depicted in Fig. 2(d). The slow space-charge wave instability is a peculiar scheme of little practical interest since it involves only a small-frequency up conversion. The nature of the interaction is not different from that of the conventional FEL instability represented by Fig. 1(a) and the other two Stokes diagram of Fig. 2(a). The fast space-charge wave instability is closely related to the beat-wave acceleration schemes discussed in Refs. 8 and 9 (it is the inverse process). It is, too, of little practical interest as an amplification mechanism, but should be of some concern, since it may be excited by a conventional FEL high-intensity signal wave which serves as a secondary pump for this instability.

#### APPENDIX B

We show that by changing the signs of all the three roots  $\delta k_i$  of the cubic Eq. (28) (this happens when the signs of the second and the fourth terms in this equation are reversed) the absolute value of  $C_s(L) / C_s(0)$  [Eq. (27)] remains unchanged. It is obvious that the multiplication factor outside the square brackets of Eq. (27) is not affected at all by changing the signs of  $\delta k_i$ , thus we have to concentrate in our discussion only on the expression given by

$$\frac{\delta k_2 - \delta k_3}{\delta k_1} e^{i\delta k_1} + \frac{\delta k_3 - \delta k_1}{\delta k_2} e^{i\delta k_2} + \frac{\delta k_1 - \delta k_2}{\delta k_3} e^{i\delta k_3} = \eta. \quad (\text{B1})$$

Because all the coefficients of the cubic equation are real, there exists only one of the possibilities<sup>14</sup> as follows:

(1) all the three roots  $\{\delta k_i\}$  are real,

(2) one root is real and the other two are complex conjugates.

(1) Assuming all roots are real, we define  $\delta k_i$  as  $x_i$  ( $i=1,2,3$ ). In that case, expression (B1) can be written in a general way as

$$\eta = a_1 e^{ix_1} + a_2 e^{ix_2} + a_3 e^{ix_3}, \quad (\text{B2})$$

where  $a_1 = (x_2 - x_3) / x_1$ ,  $a_2 = (x_3 - x_1) / x_2$ , and  $a_3 = (x_1 - x_2) / x_3$ . Equation (B2) is equivalent to

$$\eta = a_1 \cos x_1 + a_2 \cos x_2 + a_3 \cos x_3 + i(a_1 \sin x_1 + a_2 \sin x_2 + a_3 \sin x_3) \quad (\text{B3})$$

and changing the signs of  $x_i$  ( $=\delta k_i$ ) will not affect the absolute value of (B3) at all.

(2) One root is real and two are complex conjugates. We define

$$\delta k_1 = R_1 + ix_1, \quad (\text{B4})$$

$$\delta k_2 = R_1 - ix_1, \quad (\text{B5})$$

$$\delta k_3 = R_3. \quad (\text{B6})$$

Substituting into (B1) we get, after some algebraic manipulations,

$$\eta = R_T + ix_T, \quad (\text{B7})$$

$$R_T = e^{-x_1} (a_1 \cos R_1 - b_1 \sin R_1) - e^{x_1} (a_1 \cos R_1 + b_1 \sin R_1) - b_3 \sin R_3, \quad (\text{B8})$$

$$x_T = e^{-x_1} (b_1 \cos R_1 + a_1 \sin R_1) + e^{x_1} (b_1 \cos R_1 - a_1 \sin R_1) + b_3 \cos R_3, \quad (\text{B9})$$

where

$$a_1 = \frac{R_1(R_1 - R_3) - x_1^2}{R_1^2 + x_1^2} = \text{Re} \left[ \frac{\delta k_2 - \delta k_3}{\delta k_1} \right], \quad (\text{B10})$$

$$b_1 = \frac{x_1(R_3 - 2R_1)}{R_1^2 + x_1^2} = \text{Im} \left[ \frac{\delta k_2 - \delta k_3}{\delta k_1} \right], \quad (\text{B11})$$

$$b_3 = \frac{2x_1}{R_3}. \quad (\text{B12})$$

Changing the signs of  $\delta k_i$  would change the signs of  $R_1$ ,  $x_1$ , and  $x_3$  but will not affect at all the value or sign of  $a_1, b_1, b_3$ . Looking carefully at Eqs. (B8) and (B9) we see that this will transform  $R_T$  to  $-R_T$ , while  $x_T$  is not modified at all, thus the absolute value of  $\eta$  is again unchanged.

- <sup>1</sup>P. C. Liewer, A. T. Lin, and J. M. Dawson, *Phys. Rev. A* **23**, 1251 (1981).
- <sup>2</sup>J. R. Carry and J. T. Kwan, *Phys. Fluids* **24**, 729 (1981).
- <sup>3</sup>J. T. Kwan and J. R. Carry, *Phys. Fluids* **24**, 899 (1981).
- <sup>4</sup>P. C. Liewer, A. T. Lin, J. M. Dawson, and M. Z. Caponi, *Phys. Fluids* **24**, 1364 (1981).
- <sup>5</sup>A. Gover, *Opt. Commun.* **45**, 281 (1983).
- <sup>6</sup>Y. Carmel, V. L. Granatstein, and A. Gover, *Phys. Rev. Lett.* **51**, 566 (1983).
- <sup>7</sup>I. Schnitzer and A. Gover, *Nucl. Instrum. Methods Phys. Res.* (to be published).
- <sup>8</sup>M. N. Rosenbluth and C. S. Liu, *Phys. Rev. Lett.* **29**, 701 (1972).
- <sup>9</sup>Bruce I. Cohen, *Comments Plasma Phys. Controlled Fusion* **8**, 197 (1984).
- <sup>10</sup>H. Hefner, *Proc. IRE* **42**, 930 (1954).
- <sup>11</sup>A. Gover and P. Sprangle, *IEEE J. Quantum Electron.* **QE-17**, 1196 (1981).
- <sup>12</sup>A. Gover and Z. Livni, *Opt. Commun.* **26**, 375 (1978).
- <sup>13</sup>L. A. Vaynshtain, *Electromagnetic Waves* (Sovietskoye Radio, Moscow, 1957).
- <sup>14</sup>M. Abramowitz and I. Stegun, *Handbook of Mathematical Functions* (Dover, New York, 1964).
- <sup>15</sup>D. Prosnitz and A. M. Sessler, Lawrence Livermore Laboratory Report No. 86258, 1981 (unpublished).